Journal of Applied Polymer Science

Poly(vinylidene fluoride-*co*-hexafluoropropylene) Nanocomposites Incorporating Cellulose Nanocrystals with Potential Applications in Lithium Ion Batteries

Jeremiah Kelley, John Simonsen, Jie Ding
Department of Wood Science and Engineering, Oregon State University, Corvallis, Oregon 97331
Correspondence to: J. Kelley (E-mail: Jeremiah.Kelley@oregonstate.edu)

ABSTRACT: Cellulose nanocrystals (CNCs) have received considerable attention recently because CNCs can be produced from renewable materials such as straw, wood, cotton, and sea animals (tunicates). CNCs are one of the stiffest organic materials, with an estimated tensile modulus (*E*) of 80–160 GPa depending on the starting material. In addition, composites incorporating CNCs have been fabricated from a variety of polymer matrices and CNCs have been shown to increase the *E* significantly and to a lesser extent the tensile strength (TS). A copolymer of poly(vinylidene fluoride) (PVDF), PVDF-*co*-hexafluoropropylene) (PVDFHFP), has received interest over the years in the area of lithium ion battery separator technology. However, the mechanical properties of neat PVDFHFP do not meet the necessary requirements for commercial separators, especially the low *E*. In this work, novel PVDFHFP/CNC nanocomposite films were fabricated and characterized. It was found that incorporation of CNCs improves the *E* and TS. The improvement in mechanical properties of PVDFHFP upon addition of CNCs makes PVDFHFP a more suitable candidate for polymer separators in lithium ion batteries. © 2012 Wiley Periodicals, Inc. J. Appl. Polym. Sci. 000: 000–000, 2012

KEYWORDS: nanocomposites; nanoparticles; nanowires and nanocrystals; fluoropolymers

Received 25 January 2011; accepted 21 March 2012; published online
DOI: 10.1002/app.37790

INTRODUCTION

Cellulose is a linear polymer composed of glucopyranose rings linked in a β (1 $\rightarrow$ 4) fashion and is $\sim$ 70% crystalline depending on the source from which it is extracted.[1] Cellulose is the most abundant natural polymer on the planet and thus is a renewable source of filler for polymeric matrices. Cellulose is a major component of wood (50%), cotton (90%), hemp (77%), and straw (45%) and a minor component in some algae, marine animals (tunicates), and bacteria.[1,2] In the 1950s, Ränby was the first to report that sulfuric acid hydrolysis of cellulose fibers produced colloidal suspensions.[3] These particles were later termed cellulose nanocrystals (CNCs). Since the 1990s, extensive research has been carried out on the physical and chemical properties, and applications of CNCs. CNCs are long, thin rods with high aspect ratios ($\sim$ 20–100) and the final dimensions of the CNCs depend on the starting material.[2] The cellulose crystal is one of the strongest and stiffest organic materials, theoretical calculations estimate the tensile modulus (*E*) of CNCs at 80–160 GPa and an estimated tensile strength (TS) of 7.5 GPa.

CNCs have been used to fabricate nanocomposites, aerogels,[4] and hybrid materials.[5] Nanocomposites (NCs) incorporating CNCs have been fabricated using a variety of matrices; e.g., poly(vinyl alcohol) and poly(vinyl acetate),[6–8] water-borne polyurethane (WBP),[9] polypropylene,[10] starch,[11] poly(acrylic acid),[12] polyethylene oxide,[13] and low density polyethylene (LDPE).[14] In most studies, CNCs increase the *E* significantly and to a lesser extent the TS. Improvement in mechanical properties is dependent on many variables, but good dispersion of the filler in the matrix is critical.

Many fluoropolymers have been developed for a wide range of applications, for instance, the aerospace industry, architectural coatings, semiconductor manufacturing, and even photovoltaics.[15–17] These applications exploit the high strength of the carbon–fluorine bond, which gives rise to the unprecedented chemical and weathering resistance of fluoro-polymers.[16] In 1965, Arkema became the first company to produce poly(vinylidene fluoride) (PVDF) on an industrial scale marketed under the trade name Kynar.[15] PVDF is now used extensively in semiconductor manufacturing as piping and storage of high-purity

chemicals.[16] PVDF is preferred for chemical handling due to the higher crystallinity of the homopolymer compared with PVDF copolymers, because the higher crystallinity of PVDF ensures that chemical leaching is minimal.[16] A copolymer of PVDF, PVDF-*co*-hexafluoropropylene) (PVDFHFP), has gained popularity over the years in the area of lithium ion (Li^+) battery technology mainly as an electrode binder, but it has also been studied as a polymer electrolyte separator for Li^+ batteries.[18–24] However, these studies focus on improving the conductivity of PVDFHFP films by creating a porous structure using two different approaches, such as phase inversion,[21] or the Telcordia process[24] (also a phase inversion technique) rather than mechanical property improvement. Moreover, the mechanical properties of neat PVDFHFP do not meet the standard requirement for commercial separators, namely low stiffness.[24]

Commercial microporous separators are typically polyolefins.[19] The winding process by which Li^+ batteries containing microporous separator films are fabricated requires relatively high TS ($\sim$ 100 MPa) at least in the machine direction. But the key feature is that the material does not elongate during the winding process and a maximum strain of 2% at a stress of 10 MPa (for porous films rather than the neat polymer) is sufficient for most production lines.[24] According to Arora and Zhang, a more relevant material property is the E but they suggest that accurate measurement of the E is difficult due to the difficulty in determining the yield point, the point at which strain becomes irreversible.[24] In this work, novel PVDHFHFP/CNC nanocomposite films were fabricated and characterized and the improvement in mechanical properties of PVDFHFP upon addition of CNCs makes PVDFHFP a more suitable candidate for polymer separators in Li^+ batteries. This study demonstrates that it is possible to increase and control the mechanical properties of PVDFHFP films using CNCs

EXPERIMENTAL

Materials

PVDFHFP pellets (HFP content = 6%, M_n = 130,000, M_w = 400,000, melt index = 3.5–7.5 g/10 min (230°C/12.5 kg), density = 1.77 g/mL at 25°C, T_m = 140-145°C) and microcrystalline cellulose (MCC) (Avicel PH101, average particle size 50 μm) were purchased from Sigma-Aldrich, USA. *N*,*N*-Dimethylacetamide (DMAc), 98% w/w sulfuric acid, NaOH pellets, and acetone were purchased from Mallinckrodt chemicals and Selectipur LP30 electrolyte was purchased from Merck.

Sulfate CNC Production

20.0 g of MCC was hydrolyzed using 492.0 g of 64% w/w H_2SO_4 by heating at 45 °C for 1 h while stirring. After hydrolysis, the reaction mixture was diluted to 2 L, cooled to room temperature, and then centrifuged at 3500g for 1 hour. Collected pellets from centrifugation were diluted with DI water and dialyzed against about 30 gallons of DI water for 3–5 days. When the conductivity of the DI water stopped increasing the Sulfate CNC (SCNC) solution was removed from dialysis, sonicated for 1 h and then vacuum filtered to 0.7 μm through glass filter paper. After filtering, the solution was neutralized using 4*M* NaOH and re-dialyzed to remove excess salts.

SCNCs in DMAc

SCNCs were dispersed in DMAc by adding an equal amount by weight of DMAc to an aqueous SCNC solution. After the addition of DMAc, water was removed by rotary evaporation and a concentration of 0.75% SCNCs in DMAc was used to cast all composite films.

PVDFHFP/SCNC Composite Film Preparation

Control PVDFHFP films were cast from PVDFHFP in (1 : 1) acetone/DMAc at a concentration of 5% by weight using circular Petri-dishes (diameter = 70 mm). The appropriate amounts of 0.75% SCNCs in DMAc and 5% by weight PVDFHFP in acetone/DMAc were mixed in circular Petri-dishes (diameter = 70 mm) and dried under vacuum at 70°C for 24 h to obtain a composite film ($\sim$ 150 mg), and 50°C under vacuum for 4–5 h prior to electrical and mechanical testing. Acetone was used to reduce the amount of DMAc that had to be evaporated.

Analyses

All electrical measurements were carried out using a Solartron Analytical Impedance Analyzer (Hampshire, UK), consisting of a Solartron 1260 Impedance Gain-Phase Analyzer and an SI1287 Electrochemical Interface. Prior to performing electrical measurements, all aluminum electrodes and stainless steel spacers were polished using sand paper down to 10 μm (1000 grit) and sonicated between polishing steps using acetone followed by DI water to suspend removed material. After polishing, the spacers and electrodes were dried at 120°C and the polishing steps were repeated until the measured blank cell resistance was $<$500 mΩ.

Conductivity measurements of electrolyte soaked films were carried out by soaking the samples in Selectipur LP30 (conductivity = 10 mS/cm at 25°C) in a dry-box for 24 h, sandwiching the films (t = 50 μm) between two symmetric aluminum blocking electrodes (d = 1.25 cm) and measuring the impedance using impedance spectroscopy (IS) from 10 to 100 kHz with an AC amplitude of 100 mV. The conductivity (σ) was calculated from the real part of the measured impedance (Z') at the imaginary part of the impedance (Z'') = 0 using the following equation:

$$\sigma = \frac{t}{Z'A}, \tag{1}$$

where t is the film thickness and A is the area of the blocking electrodes. The blank cell resistance was measured in triplicate over the same frequency range and the average resistance of the blank was subtracted from the sample resistance before applying eq. (1). The capacitance (C) of each nonelectrolyte soaked film was measured using IS by sandwiching four films (t = 200 μm) between two symmetric aluminum blocking electrodes (d = 1.25 cm) and sweeping the frequency from 0.1 to 100 kHz with an AC amplitude of 2 V. The relative permittivities (ε_r') of the control and composite samples were calculated from the measured capacitance using the following relation:

$$C = \frac{\varepsilon_0 \varepsilon_r' A}{t}, \tag{2}$$

where A is the cross sectional area of the Al blocking electrodes, ε_0 is the permittivity of free space (8.85 pF/m), and t is the

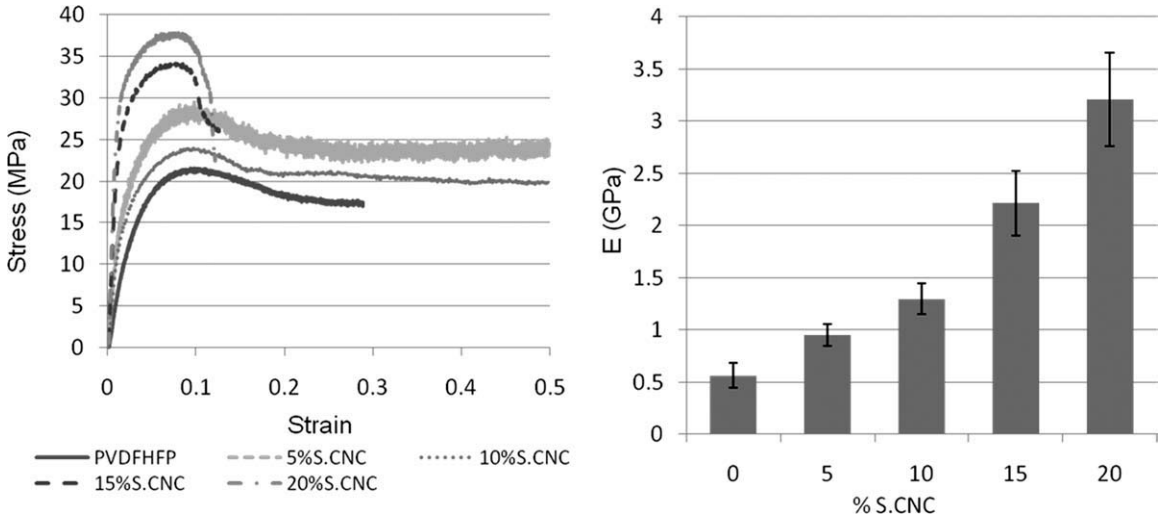

Figure 1. Stress–strain curves for PVDFHFP and PVDFHFP/SCNC composites (left); E dependence on SCNC content (right); (error bars = ±1 SD).

thickness of the film separating the electrodes. The experimental setup was validated by measuring the C of a commercially available capacitor (100 pF, RadioShack, Fort Worth, TX) and verifying that the measured C was within the listed tolerance (±5%). Further, LDPE samples cut from plastic bags (thickness ~ 30 μm) were prepared in the same way as the composite samples and used to validate the instrumental setup. This verified that the calculated ε_r' of LDPE using eq. (2) was within error of the literature value of 2.3.[1] Finally, the dissipation factor (tan δ) was calculated from the real and imaginary parts of the permittivity, ε' and ε'', respectively, from the following relationship:

$$\tan\delta = \frac{\varepsilon''}{\varepsilon'}. \tag{3}$$

Static tensile testing was performed using an Instron tensile testing machine (Norwood, MA) with an extension rate of 5 mm/min and dog-bone samples with dimensions of 0.05 mm × 30 mm × 15 mm. The work to failure (W) of the PVDFHFP/SCNC composite films were estimated by numerical integration of the stress–strain curves using the following equation:

$$W = \int \sigma d\varepsilon \tag{4}$$

where σ is stress, ε is strain, and the limits of integration are from $\sigma = 0$ to $\sigma = \sigma_b$. Dynamic mechanical analysis (Rheometrics Solid Analyzer RSA II, Richardson, TX) was performed to study the viscoelastic properties of the composite and control films around the glass transition temperature (T_g). The strain amplitude was 0.01 % at 1 Hz, and sweeps were performed from −80°C to −10°C at a heating and cooling rate of 7°C/min on rectangular samples with dimensions of 0.05 mm × 20 mm × 7 mm.

Differential scanning calorimetry (DSC) was used to determine the percent matrix crystallinity (X_c) of the control and composite samples using Al pans and a TA Instruments DSC model 2920 (New Castle, DE). DSC runs were performed over a temperature range of 30°C to 160°C using a scan rate of 10°C/min and ~5 mg samples. The enthalpy of melting (ΔH_m) was determined from DSC scans using TA Universal Analysis 2000 software. X_c was calculated using the following relationship:

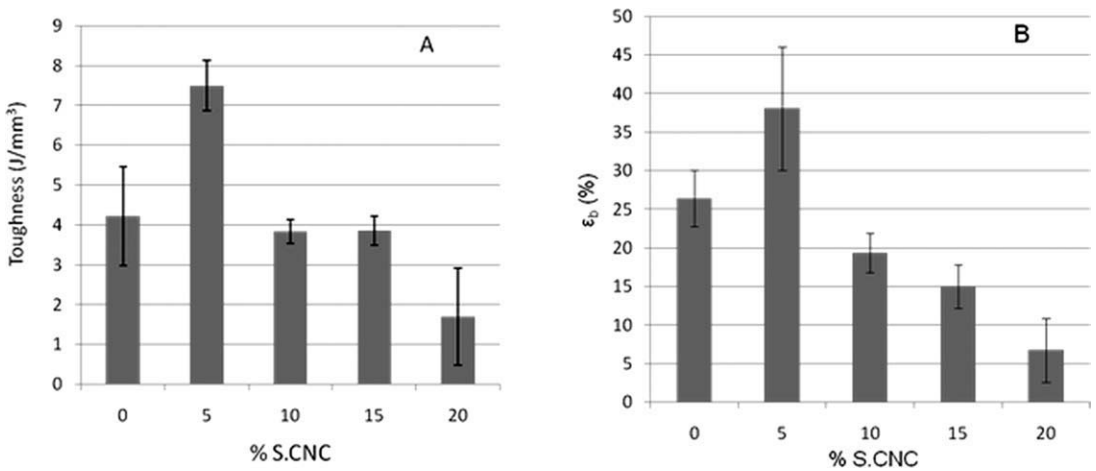

Figure 2. Work to failure (A) and ε_b (B) for PVDFHFP and PVDFHFP/SCNC composites.

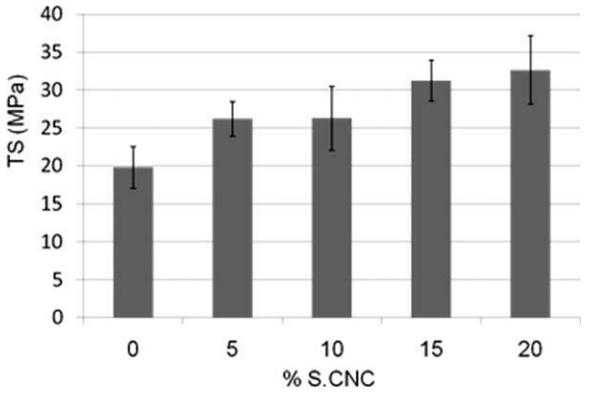

Figure 3. TS as a function of filler loading (weight %).

$$X_c = \frac{\Delta H_m}{\Delta H_{m,0}} \times \frac{100}{W_m} \quad (5)$$

where $\Delta H_{m,0}$ is the standard enthalpy of melting for PVDFHFP (104 J/g) and W_m is the weight fraction of matrix in the composite sample.[25]

RESULTS AND DISCUSSION

Tensile Testing

The stress–strain curves shown in Figure 1(A) illustrate the three observed trends in the mechanical data upon addition of SCNCs into PVDFHFP. First, the tensile modulus (E) was observed to increase with increasing SCNC loading [Figure 1(A)], which is expected because PVDFHFP is a soft matrix and SCNCs are rigid filler. Indeed, Figure 1(B) shows that the E increases for all filler loadings studied. Costa et al. reported different behavior for carbon nanofiber filled PVDF in that the E did not increase with increasing filler loading.[26] Rather the E increased drastically at low loading (0.5%) and then remained constant.[26] A possible explanation is that the higher aspect ratio (length/diameter) of carbon nanofiber (400) compared with SCNCs used in this study (20) leads to agglomeration of carbon nanofiber at lower filler loading than SCNCs.

Another trend shown in Figure 1(A) is decreasing strain at break (ε_b) with increasing SCNC loading. Figure 2 shows the calculated work to failure using eq. (4) and the experimentally determined ε_b as a function of filler loading (weight %). The ε_b decreased drastically for the highest filler loading studied (20%) but increased slightly for the 5% sample. Increases in ε_b are common in polymer composites at low filler loading, as is embrittlement at higher filler loadings. This composite system seems to follow this pattern. However, the 5% sample shows an almost twofold improvement in the work to failure and the difference is statistically significant compared with the control (t-test P value < 0.01). This is not common in macrocomposites, but has been observed in other SCNC nanocomposites.[27,28] The large decrease in the ε_b at 20% SCNC loading may be related to filler agglomeration. The major consequence of filler agglomeration is crack initiation at low stresses and rapid crack propagation through the agglomerates.

The third trend observed in Figure 1(A) is increasing TS with SCNC loading. In fact, the TS increased up to 1.7 times that of the control at 20% SCNC loading and is statistically significant compared with the control (t-test P value < 0.03) (Figure 3). In general, the improvement in the TS and E seen as a result of the addition of hydrophilic SCNCs to hydrophobic PVDFHFP is surprising and in stark contrast to other trends seen for hydrophobic polymers such as polyethylene[14] and polypropylene.[10] The mechanism of the better than expected interfacial adhesion shown here is not currently understood. The extent of reinforcement in this system is currently being evaluated using the concentric cylinder model and mean field theory and will be reported elsewhere.[29] However, PVDFHFP is soluble in a number of polar solvents, e.g., acetone, tetrahydrofuran, dimethylformamide, and *N*-methylpyrrolidone, even though it is highly hydrophobic with water absorption in the ASTM-D-570 test of 0.04%–0.07%.[15] While this water absorption value is low, it is higher than, for example, polyethylene or polytetrafluoroethylene.[1] This interesting polymer composite system deserves additional study.

Figure 4 shows the T_g determined from the maximum of the loss factor ($\tan \delta = E''/E'$) of the composite and control samples from −60°C to −20°C. It is observed that the T_g remains relatively unchanged for the composite samples compared with the control (−42°C). However, the large standard deviations obtained may mask smaller changes in the T_g. If interfacial adhesion is high in these composites, we would expect the T_g to increase with filler loading as adhesion to the filler surface restricts segmental polymer backbone motion. The T_g (−51°C) for WBP/SCNC composites decreased, however, from that of the control at 30% SCNC loading and due to the compatibility of WBP and SCNCs interfacial adhesion should be strong for WBP/SCNC composites.[9] In addition, Cao et al. observe a significant increase (>5°C) in the T_g at 30% filler loading compared with the control in plasticized starch/SCNC composites.[11] This indicates that strong interfacial adhesion could lead to promotion or restriction of polymer backbone motion depending on the nature of the matrix. This suggests that higher SCNC loading is required to achieve significant changes in the T_g for PVDFHFP.

Thermal Analysis

DSC testing indicates that matrix crystallinity (X_c) decreased from that of the control with increasing SCNC loading [Figure

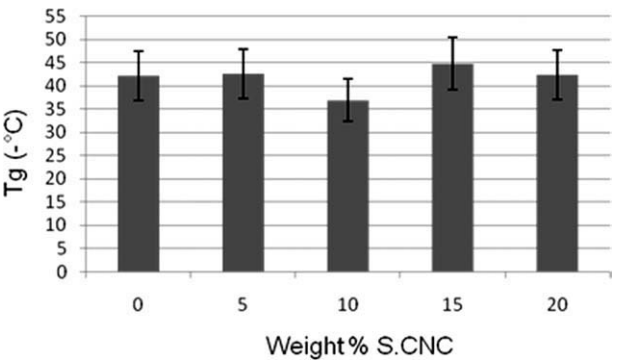

Figure 4. Glass transition temperature (T_g) dependence on filler loading.

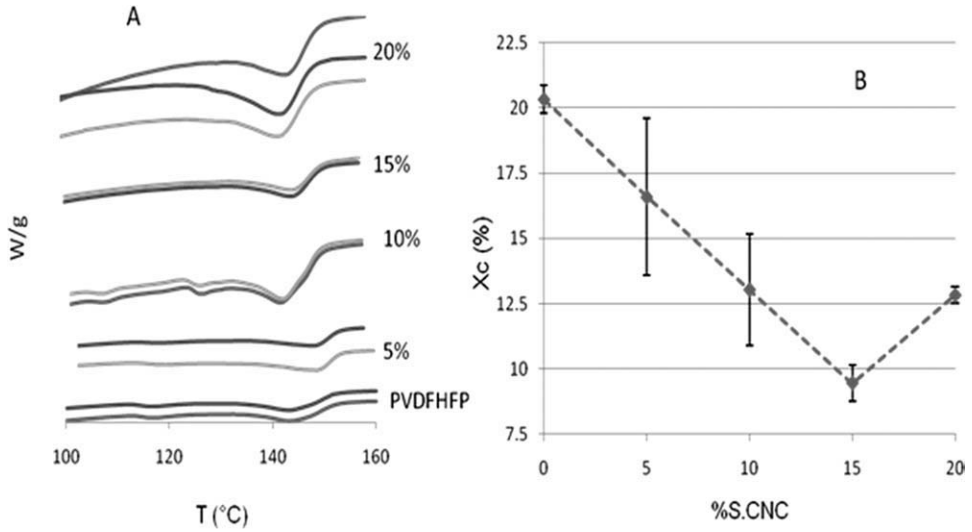

Figure 5. (A) Thermograms and (B) X_c for PVDFHFP and PVDFHFP/SCNC composites (weight %) from the first heating run. The dashed line is only an aid to viewing

5(B)]. The slight increase in X_c of the 20% sample compared with the 15% sample may be due to agglomeration, which would decrease the amount of matrix phase in contact with the SCNC surface [Figure 5(B)].

The melting temperature of the composite samples showed variable behavior which is difficult to explain [Figure 5(A)], but does not appear to be a function of filler loading. The control sample exhibits multimodal melting behavior in that the onset of melting is at 120°C and this behavior is seen only in the control and 10% SCNC composite sample. As reported in the Experimental, the casting solution was a mixture (1 : 1) of acetone and DMAc to reduce the amount of DMAc that had to be evaporated. It has been reported by Tian and Jiang,[26] that films cast from neat acetone and neat DMAc give the α and γ crystalline phases, respectively. Further, Kim et al., reported this multimodal melting behavior for PVDFHFP cast from neat NMP and it was attributed to a mixture of α and γ phases being present.[22] The similar behavior observed here for PVDFHFP/SCNC composites may be due to the α and γ phases being present as well. The two phases should not be soluble in one another and thus will give different melting points on the DSC. The decrease in X_c shown in Figure 5(B) with SCNC content (up to 15% SCNC) suggests a change in polymer morphology due to the presence of SCNCs. Similar anti-nucleation behavior has been observed for TiO_2-filled PVDFHFP by Kim et al.[22] The exact nature of these changes requires further research.

Conductivity Measurements

Considering the trend in the E and TS shown in Figures 1 and 3, the 20% sample was selected for electrolyte soaking experiments due to the improvement in the TS and the E compared

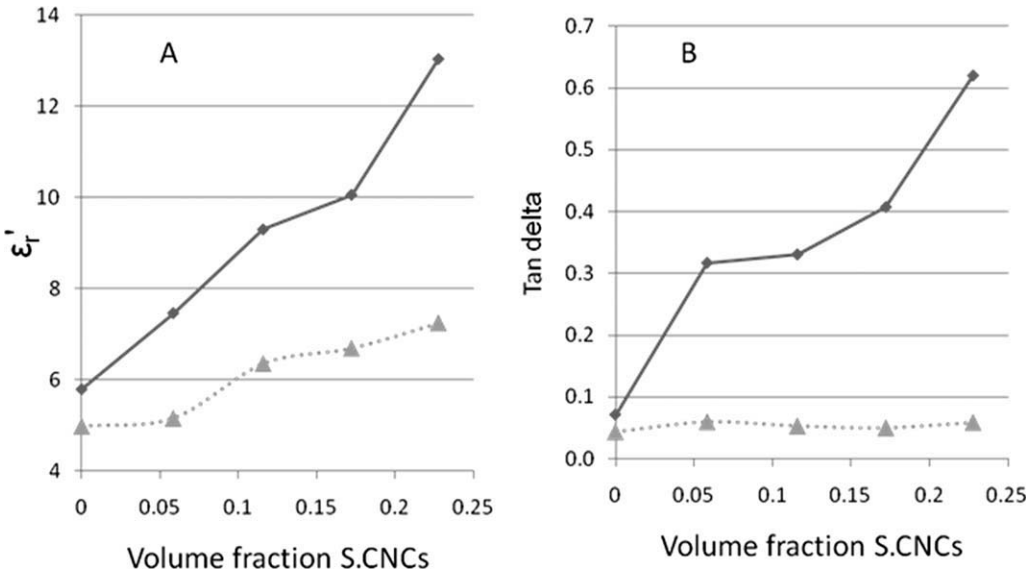

Figure 6. (A) ε_r' and (B) tan δ dependence on volume fraction of SCNCs at 100 Hz (solid) and 100 kHz (dotted).

to neat PVDFHFP. The magnitude of the room temperature conductivity (~100 μS/cm) and the % electrolyte uptake obtained for the 20% SCNC and control films (data not shown) are similar to that obtained by Kim et al. for solvent cast TiO_2/PVDFHFP nanocomposite films.[22] The low conductivity for the control and 20% samples are due to the lack of porosity in both samples (<1%) as indicated by the low % electrolyte uptake of <100%. Unexpectedly, the addition of SCNCs does not affect electrolyte uptake compared with the control even at 20% SCNC loading. The unchanged electrolyte uptake is likely due to the decreased matrix crystallinity at 20% filler loading [Figure 5(B)] since the crystalline phase should not absorb electrolyte.

Permittivity Measurements

In an attempt to better understand the nature of the interactions between SCNCs and PVDFHFP, the relative permittivities (ε_r') for the control and composite samples were calculated from the measured capacitances (C) using eq. (2). Figure 6(A) shows the ε_r' at 0.1 and 100 kHz and it is observed that the ε_r' of the composite films increased with filler loading.

The behavior of ε_r' versus filler loading seen here is similar to that observed for barium titanate (BT)/PVDFHFP composites in that the ε_r' increases with increasing filler loading and the increases in ε_r' for PVDFHFP/SCNC composites are comparable to that achieved using high ε_r' BT at the same filler loading.[30,31] The behavior shown here for tan δ [Figure 6(B)]; however, is drastically different for PVDFHFP/SCNC composites compared with BT/PVDFHFP composites. Kim et al.[30,31] report that tan δ decreases with increasing filler loading, suggesting that the counterions (e.g., Na^+) present in SCNC/PVDFHFP composites are acting as polarizable moieties and thus increasing tan δ at 100 Hz. At 100 Hz, the data suggest that the charged SCNC surface contributes to increases in (1) the orientational polarization of the composite films compared with the control thus contributing to the increased ε_r' values and (2) ionic polarization which causes tan δ to increase drastically at 100 Hz [Figure 6(B)]. At 100 kHz, the frequency is evidently greater than the relaxation time of the dipoles as both the ε_r' and tan δ are greatly reduced from their low frequency values.

CONCLUSIONS

As shown in Figures 1(B) and 3, the increase in the modulus and TS of the 20% composite film could prove useful in a variety of applications. One application could be separators for Li^+ batteries, but further studies are needed on porous films. Also, additional testing to determine (once porous films are obtained) the shutdown performance and dendrite resistance would help to evaluate the suitability of these composites for battery applications. The low TS of PVDFHP/SCNC composites in comparison with ultra-high molecular weight polyethylene may be detrimental to the use of these films in commercial Li^+ batteries produced by high speed winding. Porous films would be expected to show even lower mechanical properties than the films studied here. However, additional testing is needed to evaluate how the presence of pores will affect the properties. Most studies of Li^+ battery separators focus on increasing the conductivity of separator films rather than mechanical property improvement. However, the use of films for separators does require that some minimal criteria of mechanical properties be met. The large increase in the E at 20% SCNC loading ensures that the decreased E due to the presence of pores will still be an improvement relative to neat PVDFHFP at 20% SCNC loading. Finally, this study demonstrates that it is possible to increase and control the mechanical properties of PVDFHFP films using SCNCs, but the utility of this new knowledge requires further study before any commercialization potential can be evaluated.

ACKNOWLEDGMENTS

The authors thank the Oregon Nanoscience and Microtechnologies Institute (ONAMI) for funding through ONAMI Gap and US Army Tactical Energy Systems funding Programs. In addition, the authors thank Dr. Mike Lerner for access and training on equipment in his lab.

REFERENCES

1. Mark, J. E., Ed. Polymer Data Handbook. Oxford University Press: West Sussex, England, **1999.**
2. Habibi, Y.; Lucia, L. A.; Rojas, O. *J. Chem. Rev.* **2010,** *110*, 3479.
3. Ränby, B. G. *Discuss. Faraday Soc.* **1951,** *11*, 158.
4. Capadona, J. R.; Van Den Berg, O.; Capadona, L. A.; Schroeter, M.; Rowan, S. J.; Tyler, D. J.; Weder, C. *Nat. Nanotechnol.* **2007,** *2*, 765.
5. Mangalam, A. P.; Simonsen, J.; Benight, A. S. *Biomacromolecules* **2009,** *10*, 497.
6. Roohani, M.; Habibi, Y.; Belgacem, N. M.; Ebrahim, G.; Karimi, A. N.; Dufresne, A. *Eur. Polym. J.* **2008,** *44*, 2489.
7. Qua, E. H.; Hornsby, P. R.; Sharma, H. S. S.; Lyons, G.; McCall, R. D. *J. Appl. Polym. Sci.* **2009,** *113*, 2238.
8. Lis, N.; de Rodriguez, G.; Thielemans, W.; Dufresne, A. *Cellulose* **2006,** *13*, 261.
9. Cao, X.; Dong, H.; Ming Li, C. *Biomacromolecules* **2007,** *8*, 899.
10. Ljungberg, N.; Bonini, C.; Bortolussi, F.; Boisson, C.; Heux, L.; Cavaille, J. Y. *Biomacromolecules* **2005,** *6*, 2732.
11. Cao, X.; Chen, Y.; Chang, P. R.; Muir, A. D.; Falk, G. *Express Polym. Lett.* **2008,** *2*, 502.
12. Lu, P.; Lo Hsieh, Y. *Nanotechnology* **2009,** *20*, 1.
13. Samir, M. A. S. A.; Alloin, F.; Gorecki, W.; Sanchez, J. Y.; Dufresne, A. *J. Phys. Chem. B* **2004,** *108*, 10845.
14. de Menezes, A. J.; Siqueria, G.; Curvelo, A. A. S.; Dufresne, A. *Polymer* **2009,** *50*, 4552.
15. Kynar.com; accessed May 11.
16. Scheirs, J., Ed. Modern Fluoropolymers. Wiley: London, England, **1997.**
17. Mu Leea, K.; Suryanarayananb, V.; Chuan Hoc, K. *J. Photochem. Photobiol. A: Chem.* **2009,** *207*, 224.
18. Walkowiak, M.; Zalewskab, A.; Jesionowski, T.; Waszak, D.; Czajka, B. *J. Power Sources* **2006,** *159*, 449.

19. Ahmad, S. *Ionics* **2009,** *15*, 309.

20. Xie, H.; Tang, Z.; Li, Z.; He, Y.; Liu, Y.; Wong, H. *J. Solid State Electrochem.* **2008,** *12*, 1497.

21. Stephan, A. M.; Nahm, K. S.; Kumarm, T. P.; Kulandainathan, M. A.; Ravi, G.; Wilson, J. *J. Power Sources* **2006,** *159*, 1316.

22. Kim, K. M.; Park, N. G.; Ryua, K. S.; Changa, S. H. *Electrochim. Acta* **2006,** *51*, 5636.

23. Du Pasquier, A.; Warren, P. C.; Culver, D.; Gozdz, A. S.; Amatucci, G. G.; Tarascon, J. M. *Solid State Ionics* **2000,** *135*, 249.

24. Arora, P.; Zhang, Z. *Chem. Rev.* **2004,** *104*, 4419.

25. Tian, X.; Jiang, X. *J. Hazard. Mater.* **2008,** *153*, 128.

26. Costa, P.; Silva, J.; Sencadas, V.; Costa, C. M.; van Hattum, F. W. J.; Rocha, J. G.; Lanceros-Mendez, S. *Carbon* **2009,** *47*, 2590.

27. Choi, Y. A.; Simonsen, J. *J. Nanosci. Technol.* **2006,** *6*, 633.

28. Noorani, S.; Choi, Y. A.; Simonsen, J. *Cellulose* **2007,** *14*, 577.

29. Moon, R.; Martini, A.; Nairn, J.; Simonsen, J.; Youngblood, J. *Chem. Soc. Rev.* **2011,** *40*, 3941.

30. Kim, P.; Jones, S. C.; Hotchkiss, P. J.; Haddock, J. N.; Kippelen, B.; Marder, S. R.; Perry, J. W. *Adv. Mater.* **2007,** *19*, 1001.

31. Kim, P.; Doss, N. M.; Tillotson, J. P.; Hotchkiss, P. J.; Jen Pan, M.; Marder, S. R.; Li, J.; Calame, J. P.; Perry, J. W. *ACS Nano.* **2009,** *3*, 2581.